Available online at www.sciencedirect.com

SCIENCE DIRECT®

Vision Research 45 (2005) 1725–1743

Vision Research

www.elsevier.com/locate/visres

Laminar cortical dynamics of 3D surface perception: Stratification, transparency, and neon color spreading

Stephen Grossberg *, Arash Yazdanbakhsh [1]

Department of Cognitive and Neural Systems and Center for Adaptive Systems, Boston University, 677 Beacon Street, Boston, MA 02215, United States

Received 30 January 2004; received in revised form 16 November 2004

Abstract

The 3D LAMINART neural model is developed to explain how the visual cortex gives rise to 3D percepts of stratification, transparency, and neon color spreading in response to 2D pictures and 3D scenes. Such percepts are sensitive to whether contiguous image regions have the same contrast polarity and ocularity. The model predicts how like-polarity competition at V1 simple cells in layer 4 may cause these percepts when it interacts with other boundary and surface processes in V1, V2, and V4. The model also explains how: the Metelli Rules cause transparent percepts, bistable transparency percepts arise, and attention influences transparency reversal.

Keywords: Surface perception; Perceptual grouping; 3D figure-ground separation; Transparency; Neon color spreading

1. Introduction

1.1. Depthful grouping of 2D cues

Refinement of the 3D LAMINART model (Fig. 1) enables it to simulate percepts of transparency (Fig. 2) and neon color spreading (Fig. 3). These percepts can be influenced by changing how 2D information is combined from both eyes and by changing the contrast relationships in a 2D picture without changing the geometrical layout of its edges. Such variations provide important clues to how the brain carries out normal 3D vision. Sections 2 and 3 summarize challenging data about these percepts. They are then explained and simulated as emergent properties of all model stages interacting together. Previous versions of the model have clarified how cortical areas V1, V2, and V4 work together to generate other percepts (Grossberg, 1999a, 1999b, 2003; Grossberg & Howe, 2003; Grossberg & Raizada, 2000; Grossberg & Seitz, 2003; Grossberg & Swaminathan, 2004; Grossberg & Williamson, 2001; Raizada & Grossberg, 2003). The model refinement is needed to extend the model's predictive range to explain the targeted data. This refinement predicts that inhibitory interneurons within layer 4 of V1 prefer to contact cells that are sensitive to the same contrast polarity. This affinity can be explained by models of cortical development (Grossberg & Williamson, 2001), but its implications for perception were previously unclear. The results have been briefly reported in Grossberg and Yazdanbakhsh (2003a, 2003b).

1.2. Contrast relationships that induce transparency

Many researchers have noted how contrast relations within an image can cause or eliminate a percept of transparency (Adelson, 2000; Anderson, 1997; Beck,

* Corresponding author. Tel.: +1 617 353 7858; fax: +1 617 353 7755.
E-mail address: steve@bu.edu (S. Grossberg).

[1] Authorship in alphabetical order. SG was supported in part by the Air Force Office of Scientific Research (AFOSR F49620-01-1-0397), the National Science Foundation (NSF SBE-0354378), and the office of Naval Research (ONR N00014-01-1-0624). AY was Supported in part by the Office of Naval Research (ONR N00014-01-1-0624).

0042-6989/$ - see front matter © 2005 Elsevier Ltd. All rights reserved.
doi:10.1016/j.visres.2005.01.006

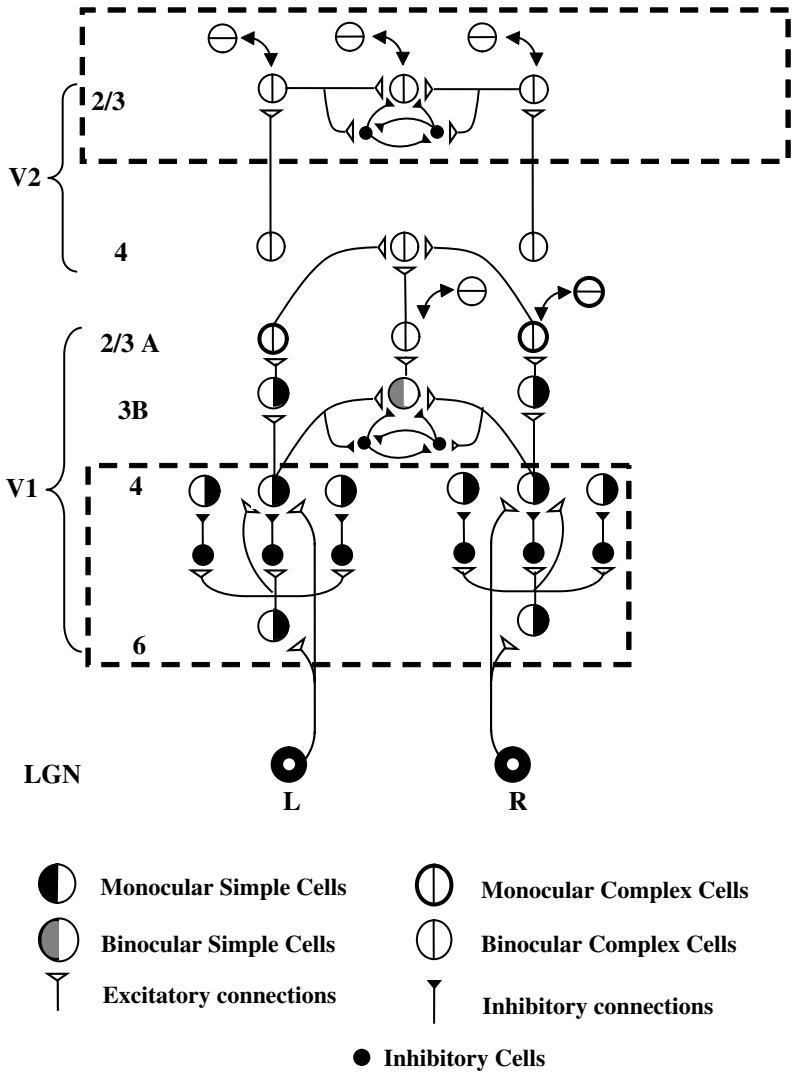

Fig. 1. 3D LAMINART model: before layer 3B of V1, the cells and their connections are eye specific. Like-polarity spatial competition in layer 4 implements the monocular contrast process. Long-range boundary grouping in layer 2/3 of V2 is both binocular and contrast invariant, because opposite eye streams have already been pooled in layer 3B of V1 and layer 4 of V2, and opposite contrasts have already been pooled in layer 2/3 of V1. These laminar circuits clarify how both contrast-polarity sensitive and contrast-polarity pooling processes can coexist together. In the upper dashed box of the figure, a set of vertically-oriented bipole cells are shown, each of them belongs to a group of colinear vertically-oriented bipole grouping cells.

Prazdny, & Ivry, 1984; Metelli, 1974; Watanabe & Cavanagh, 1993a, 1993b). The images in Fig. 2 all have the same edge geometry (Fig. 2d); however, we perceive them differently. The contrast relations at the figures' X-junction determine the percept. In Fig. 2a, the bottom square is perceived as a transparent layer over the top square. The opposite percept, with the bottom square being over the top one, does not occur. Here contrast polarity (dark-light versus light-dark) is preserved along the vertical branch of the X-junction. Moreover, this X-junction branch is part of a surface that is partially occluded by the transparent layer that is attached to the polarity-reversing edge. In Fig. 2b, either square can be seen as a transparent surface over the other one. Here contrast polarity is preserved along both X-junction branches, and the percept is bistable. Fig. 2c does not induce a percept of transparency. Here polarity-reversal takes place along both branches. Depth stratification does not occur. Instead, the image looks like a bright small square in the middle that is surrounded by two dark L-shaped figures.

These displays show that the relative contrasts at aligned edges of contiguous regions influence whether a transparency percept is perceived. The same contrast polarity at aligned edges of contiguous regions facilitates transparency, whereas opposite contrast polarities prevent transparency. Sensitivity to contrast polarity suggests an influence from an early stage of cortical processing, notably V1. We are therefore led to ask: How does polarity-sensitive V1 processing alter the 3D per-

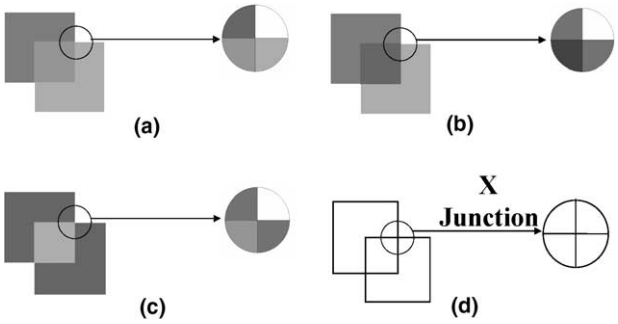

Fig. 2. The correspondence between polarity alignment and the presence or absence of transparency: each panel shows the specific contrast relationship that favors or does not favor transparency. (a) Single polarity reversal favors unique transparency. (b) No polarity reversal favors bistable transparency. (c) Double polarity reversal does not support transparency. (d) All of these images have the same geometry of edges.

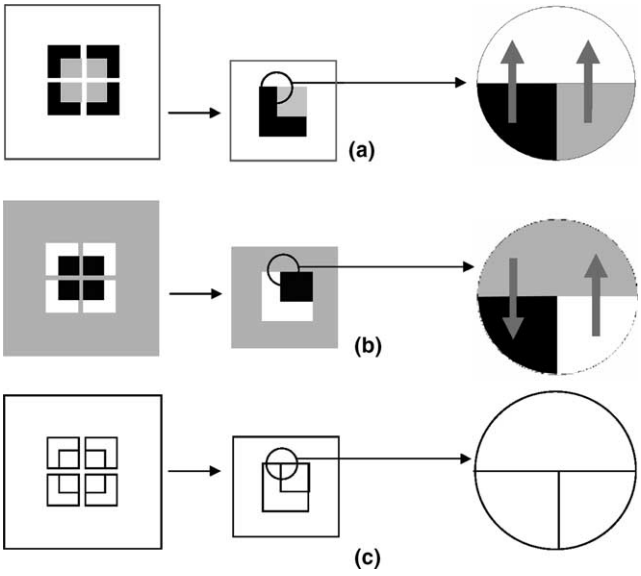

Fig. 3. (a) Like-polarity contrasts favor neon color spreading: the T-junction is polarity preserving. (b) Opposite contrast polarities block neon color spreading: the T-junction is polarity reversing. (c) In both (a) and (b), the edge geometry, including all T-junctions, is the same.

ceptual groupings that occur in V2, and thus the visible 3D surface percepts that occur in V4?

1.3. Contrast relationships that induce neon color spreading

The different panels of Fig. 3 also have the same edge geometry but different contrast relationships again induce different percepts. Neon color spreading occurs when the contrast polarity along the T-junctions is preserved (Fig. 3a). Neon is abolished when the polarity along the T-junctions reverses (Fig. 3b). The influence of like-polarity contrast relations in neon color spreading also implicates early stages of V1 cortical processing.

1.4. Ocularity of contrast relations in neon color spreading

Takeichi, Shimojo, and Watanabe (1992) showed that the contrast polarity constraint that determines neon color spreading is monocular (Fig. 4). Fusing the stereogram in Fig. 4a, results in a percept of neon color spreading bounded by an illusory square. However, fusing the stereogram in Fig. 4b does not result in neon color spreading. The contrast relation that favors neon spreading thus needs to be present completely in one eye. We localize this constraint to layer 4 of cortical area V1, as indicated below.

1.5. Contrast-polarity sensitivity versus contrast-polarity pooling

Another constraint on contrast polarity further localizes the monocular contrast constraint, but seems at the outset to be at odds with it. Fig. 5 illustrates that perceptual boundaries can form around objects in front of textured backgrounds. To achieve this, the boundary grouping process pools signals from opposite contrast

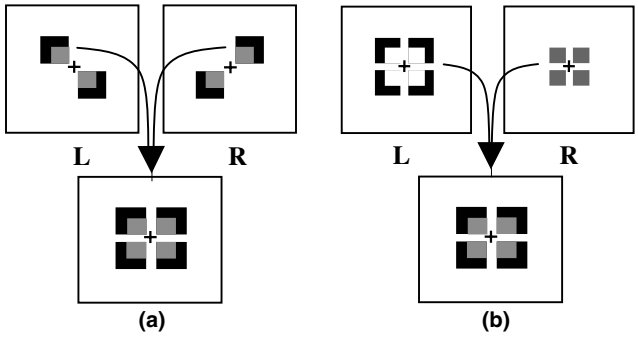

Fig. 4. (a) Splitting the inducers from Fig. 2a across two eyes, while preserving the contrast relations within each eye, elicits neon color spreading. The illusory square bridges different ocularities. (b) When the contrasts of Fig. 2a are split between the two images of the stereogram, then fusion of the stereogram does not yield neon color spreading.

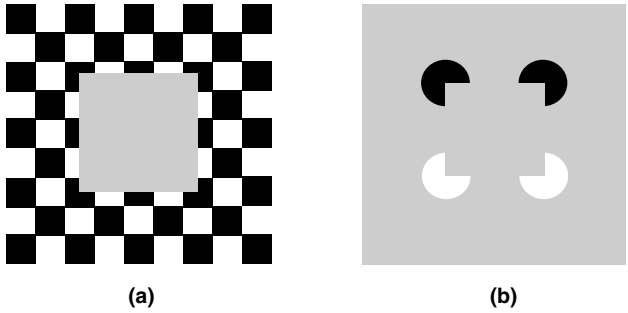

Fig. 5. (a) Boundary formation is contrast invariant: the polarity of contrasts along the square boundary reverses. However, these opposite contrasts are pooled by the brain to form the object boundary. (b) Long-range grouping to form the Kanizsa square pools over opposite contrast polarities.

polarities at each position (Grossberg, 1994; Grossberg & Mingolla, 1985a, 1985b). In other words boundary grouping is *contrast-polarity invariant*.

How does the brain reconcile the coexistence of contrast-polarity sensitivity with contrast-polarity pooling for boundary formation? The 3D LAMINART model (Fig. 1) unifies and functionally interprets many anatomical and neurophysiological data (Table 1), notably data concerning the laminar organization of V1 and V2, to propose an explanation of the data targeted in this paper. The model proposes that contrast-invariant pooling occurs in layer 2/3A of V1 (Table 1, row 12) after like-polarity binocular fusion occurs in layer 3B (Fig. 1; Table 1, rows 11 and 13).

1.6. Locating the monocular contrast constraint in V1 layer 4: A key prediction

Since V1 cells in layer 3B have already lost ocularity and are influenced by both eyes, we predict that the polarity-specific monocular process occurs before layer 3B of V1, notably in layer 4, where it can discriminate between the split contrast and the non-split contrast constraints in Takeichi et al. (1992). The next sections

Table 1
Neurophysiological and anatomical evidence for LAMINART

	Connection in model (all in V1 unless otherwise noted)	Functional interpretation	Selected references
1	LGN → 4	Strong, oriented LGN input	Blasdel and Lund (1983), Ferster et al. (1996, cat)
2	LGN → 6	LGN input sharpened by 6 → 4 on-center off-surround	Blasdel and Lund (1983)
3	6 → 4 spiny stellates	Modulatory on-center of the 6 → 4 on-center off-surround	Stratford et al. (1996, cat), Callaway (1998)
4	6 → 4 inhibitory interneurons	Off-surround of the 6 → 4 on-center off-surround	McGuire et al. (1984, cat), Ahmed et al. (1997, cat)
5	4 inhibitory interneurons. → 4 inhibitory interneurons	Context-dependent normalization of off-surround inhibition	Ahmed et al. (1997, cat), Tamas et al. (1998, cat)
6	4 → 2/3 pyramidals	Feedforward of stimuli with bottom-up support	Fitzpatrick et al. (1985), Callaway and Wiser (1996)
7	2/3 pyramidals → 2/3 pyramidals	Long-range collinear integration along RF axes	Bosking et al. (1997, shrew), Schmidt et al. (1997, cat), Tucker and Katz (2003a, 2003b, ferret)
8	2/3 pyramidals → 2/3 inhibitory interneurons	Keep outward grouping subthreshold (bipole property)	McGuire et al. (1991), Hirsch and Gilbert (1991, cat), Tucker and Katz (2003a, 2003b, ferret)
9	2/3 inhibitory interneurons → 2/3 inhibitory interneurons	Normalize 2/3 inhibition (2-against-1 part of bipole property)	Tamas et al. (1998, cat), Tucker and Katz (2003a, 2003b, ferret)
10	V1 2/3 pyramidals → V2 layer 4	Feedforward of V1 groupings into V2	Van Essen et al. (1986), Rockland and Virga (1990)
11	Presence of simple cells and binocular cells in layer 3B of V1	Contrast sensitivity in layer 3B and obligate property	Dow (1974), Hubel and Wiesel (1968), Poggio (1972), Katz et al. (1989)
12	3B → 2/3 in V1 and the presence of binocular and complex cells in layer 2/3	Pooling responses of layer 2/3 of both contrast polarity from layer 3B	Callaway (1998), Poggio (1972)
13	Presence of cells in layer 3B and 2/3 that exclusively respond to binocular, not monocular stimulation	Obligate property	Poggio and Fischer (1977, rhesus), Smith et al. (1997), Poggio and Talbot (1981, rhesus), Poggio (1991)
14	Presence of monocular cells in layers 2 and 3	V1 monocular boundary formation	Poggio (1972), Hubel and Wiesel (1968)
15	V2 cells are mostly binocular	Model V2 cells (layer 4) input from both ocularities of monocular V1 cells (layer 2/3)	Hubel and Livingstone (1987), Roe and Ts'o (1997)
16	V2 cells are disparity–sensitive	Depth detection in V2	Poggio and Fischer (1977, rhesus), von der Heydt et al. (2000), Peterhans (1997)
17	No false matches in V2	Disparity filter in V2	Bakin et al. (2000)
18	Presence of false matches in V1	Depth propagation in model V1	Cumming and Parker (2000)
19	Presence of many complex cells in V2	Exclusive implementation of complex cells in the model V2	Hubel and Livingstone (1987)

show that this polarity-specific monocular process is *monocular like-polarity competition*.

2. 3D LAMINART circuit

Fig. 1 summarizes how monocular polarity-specific competition is realized within the 3D LAMINART model. See the V1 circuit surrounded by the dashed line in Fig. 1. Like-polarity binocular fusion occurs at binocular simple cells in layer 3B of V1 (Table 1, rows 11 and 13). Pooling of opposite contrast polarities occurs at complex cells in V1 (Table 1, row 12). Monocular and binocular signals are pooled at layer 4 of V2 (Table 1, row 15). A disparity filter also occurs in V2 to help solve the correspondence problem (Table 1, rows 16 and 17). Long-range contrast-invariant boundary completion, as in the Kanizsa square percept of Fig. 5b, occurs in layer 2/3 of V2; see the V2 circuit surrounded by the dashed line in Fig. 1 and Table 1 (rows 7, 8, and 9).

3. Contrast influences both boundary and surface processing

Because contrasts are pooled to form long-range boundary groupings (Fig. 5b), thereby eliminating the possibility of distinguishing dark from light, they do not generate a visible percept within the boundary grouping system. Visibility is predicted to be a property of the surface filling-in system (Grossberg, 1994; Grossberg & Mingolla, 1985b). Interactions between the boundary and surface systems lead to the visible 3D surface percepts that are explained herein. An early stage in this interaction uses the depth-selective binocular boundaries that are formed in layer 2/3A of V2 (Fig. 1) to selectively capture monocular surface signals at their depth (Fig. 6, pathways 6). This surface capture process leads to a final percept of surfaces seen at different depths in V4. How this happens is described elsewhere to explain other data; e.g., Grossberg (1994, 1997, 2003), Grossberg and Swaminathan (2004) Kelly and Grossberg (2000). Here we review properties that are needed to explain the present data.

One such property is that the illuminant is discounted (Fig. 6, LGN stage) before the stage of depthful surface capture (Fig. 6, Monocular Surfaces stage). This discounting process suppresses lightness and color signals within the interiors of regions with nearly uniform achromatic or chromatic contrast across space (Fig. 7a). Contrasts are computed, with the illuminant discounted, at positions of rapid contrast change (Fig. 6, LGN stage). These contrasts then fill-in surface regions within boundaries that inhibit, or gate, their spread (Fig. 6, Monocular Surfaces stage). If the boundary corresponding to a surface border forms a closed contour, then it

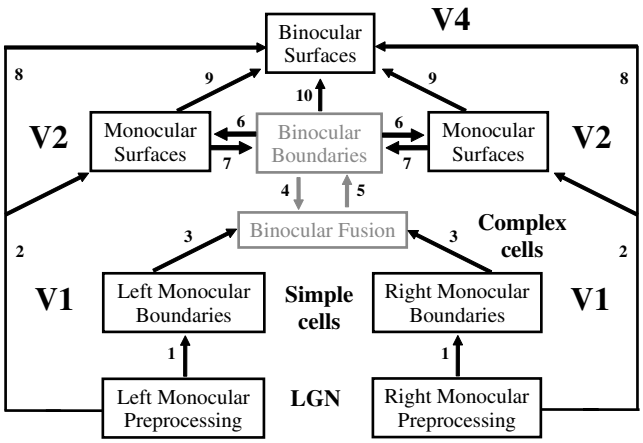

Fig. 6. In FACADE theory, the illuminant-discounted inputs from right and left monocular preprocessing stage, which is composed of center-surround cells, output to the left and right monocular boundaries composed of simple cells via pathway 1. This is the place where we suggest that like-polarity competition occurs (See Fig. 1, V1 layer 4). Via pathways 3, left and right monocular boundaries are binocularly fused and through feedback via pathways 4 and 5 incorporate bipole long-range grouping which is provided by the binocular boundaries stage. Depthful binocular boundaries mutually interact with the monocular surfaces stage (pathways 6), where the closed boundaries are filled-in by the illuminant-discounted surface input. The attached boundaries to the successfully filled-in surfaces prune the corresponding boundaries at the farther depths at the same spatial positions (pathways 7). In the binocular surfaces stage, inputs from the left and right monocular preprocessing stages, and also the left and right monocular surface stages, are matched binocularly (pathways 8 and 9). The former match is based on excitatory inputs to the binocular surfaces stage and the latter match is inhibitory and carries out surface pruning. Binocular boundaries are added to the same positions from near depths to far depths (pathways 10) to realize boundary enrichment. Due to surface pruning, the illuminant-discounted surface inputs associated with the enriched boundaries are pruned from the depths where boundaries are added (Pathway 9). The simulations in Figs. 12 and 15 illustrate how these processing stages work.

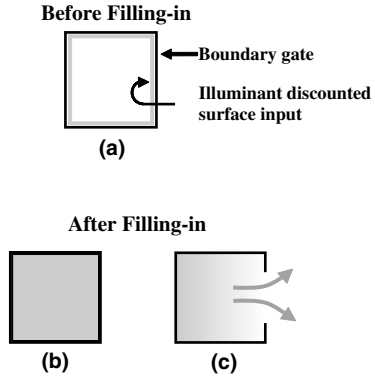

Fig. 7. Each boundary output to the surface system is accompanied by illuminant-discounted surface inputs which estimate the contrast magnitude across the corresponding edge. (a) Before filling-in. (b) If the boundary does not have a gap, it then can contain filling-in and may lead to a visible surface percept. (c) A boundary with gap lets the filling-in dissipate, thereby preventing a visible surface percept.

can contain the filling-in of surface lightness and color (Fig. 7b). If the boundary has large gaps, then surface lightness and color can dissipate by spreading through the gaps (Fig. 7c), thereby initiating the separation of surfaces in depth. We show how this happens by combining circuits in Figs. 1 and 6 to explain the targeted data. The 3D LAMINART system (Fig. 1) realizes the following stages in Fig. 6: Left and Right, Monocular Preprocessing (Fig. 1, LGN), Left and Right, Monocular Boundaries (Fig. 1, Layers 6 to 2/3A leading to Monocular Complex Cells), Binocular Fusion (Fig. 1, Binocular Simple Cells and Complex Cells) and Binocular Boundaries (Fig. 1, V2). The larger FACADE (Form-And-Color-And-DEpth) system in Fig. 7 joins together boundary and surface processing.

4. How do surfaces and boundaries interact to cause transparency?

FACADE theory explains why a surface with a connected boundary is represented at a nearer depth than one with a boundary gap (Fig. 8a): in response to viewing a 2D picture, the same boundaries initially form in several depth planes (Fig. 9a) due to the size-disparity correlation (Kulikowski, 1978; Richards & Kaye, 1974; Schor & Tyler, 1981; Schor & Wood, 1983; Schor, Wood, & Ogawa, 1984; Tyler, 1975, 1983). A closed connected boundary in the BCS can contain filling-in within its surface region. A contrast-sensitive network is activated at the edges of such a filled-in region. This network sends feedback from surfaces to boundaries. The feedback is *positive* to the boundary at its own position and depth and *negative* to boundaries at the same positions but further depths (Fig. 9b). Surface-to-boundary feedback confirms and strengthens the boundary that formed the surface region, while it inhibits, or prunes, any extra boundaries that form (Fig. 9b). It hereby assures the consistency of boundary and surface representations.

When the boundaries of a near surface are inhibited at a far depth (Fig. 9b), the boundary gaps at the far depth can be removed by collinear grouping, and the resultant closed boundary can contain surface filling-in of its illuminant-discounted input contrasts. In Fig. 9b, the filled in surfaces at the near and far depths overlap, which corresponds to a percept of transparency.

The separated and completed boundaries and surfaces at the Monocular Surfaces stage in V2 enable us to recognize partially occluded objects. If these monocular surfaces were the ones that we see, however, then all occluders would look transparent (Grossberg, 1994). Visible 3D percepts are predicted to form at the Binocular Surfaces stage in V4 (Fig. 6). The model hereby clarifies how the brain can *recognize* objects that are partially occluded by opaque objects, even though we can *see* only the unoccluded parts of these objects. It also explains when objects do look transparent. The distinction between seeing and recognizing is achieved by two mechanisms that act together: (1) adding boundaries at V2 to the surface representations at all further depths in V4 (*boundary enrichment*; pathways 10 in Fig. 6); and (2) inhibiting monocular surface inputs to the surface representations at these farther depths (*surface pruning*; path-

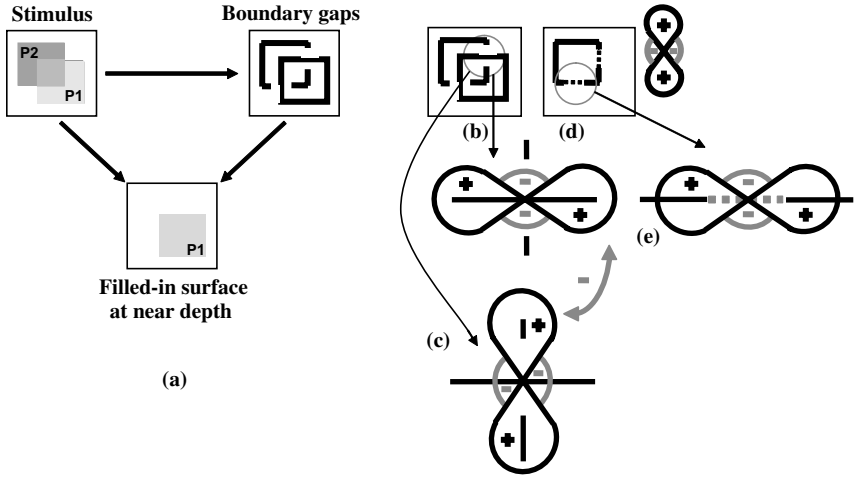

Fig. 8. (a) In response to the stimulus, the intact boundary keeps its surface at the near depth and the surface presentation of the broken boundary will be forced behind (see Fig. 9). How boundary gaps are generated and repaired: Panel (b) shows that in unique transparency, the underneath surface boundaries get gaps (within the circle) and as soon as the boundary signals across the gaps are pruned, the gaps can be repaired (see inside the circle). Panel (c) zooms into the circle region of panel (b) to show how gaps can be created: the bipole grouping cells with different orientation preference (here orthogonal) compete. The stronger bipole inhibits the weaker bipole through orientational competition and causes gaps. The circle zone in (d) can be repaired because both lobes of bipole grouping cells get input (e). Before boundary pruning, the orthogonal boundary signal across the gap blocks the bipole grouping (b) both due to the activation of the inhibitory part of the bipole and also orientational competition as in (c).

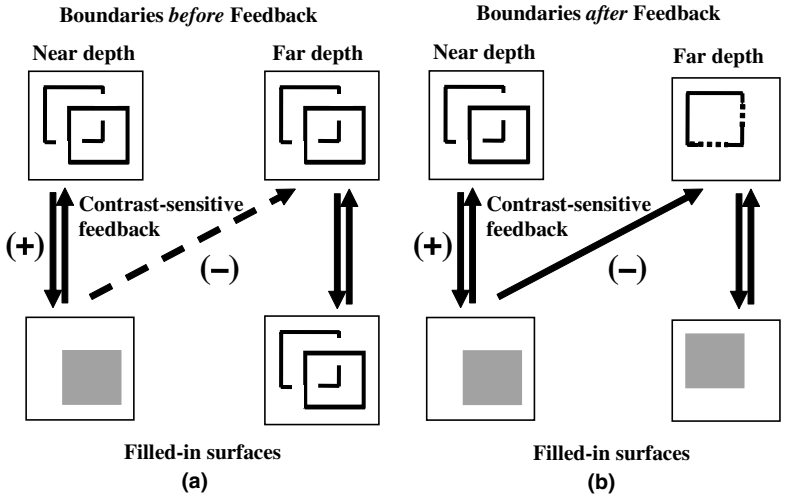

Fig. 9. (a) Upper row shows that the initial boundary grouping is redundantly represented at several depths due to the size-disparity correlation. The successfully filled-in region will be assigned to the nearest depth that can create a closed connected boundary. Further boundaries at these positions are inhibited by contrast-sensitive topographic feedback from the successfully filled-in surface region. (b) Contrast-sensitive inhibitory feedback prunes the boundaries at further depths while strengthening the successfully filled-in boundaries at the near depth. Gaps in the occluded boundaries can then be repaired by collinear grouping.

way 9 in Fig. 6). As discussed below (Figs. 12 and 15), these processes do not change the V2 boundaries and surfaces that form in the transparency and neon cases.

5. How are boundary gaps created and repaired?

Section 4 summarized how boundary gaps can lead to a transparent surface percept. Now we discuss how the monocular like-polarity competition enables these gaps to form, and how they are repaired. Perceptual grouping takes place in layer 2/3 of V2. The *bipole property* of such groupings can both generate boundary gaps and repair them by using a combination of long-range excitatory horizontal connections and short-range disynaptic inhibitory connections (Fig. 1). The excitatory connections converge on a bipole cell from opposite sides, and enable it to complete illusory contours at positions that receive no bottom-up input. The inhibitory connections prevent such a boundary from forming unless there is convergent excitatory input from both sides. These inhibitory interactions also compete with boundaries that are trying to form with different, notably perpendicular, orientations at the same position. We will see below how monocular like-polarity competition assures that the boundaries of the rightmost square in Fig. 8b are stronger than those of the leftmost square. After competition across orientation (Fig. 8c), the boundaries of the leftmost square are broken (Fig. 8b). When contrast-sensitive surface-to-boundary feedback prunes the redundant boundaries of the rightmost square at the far depth (Fig. 9b, far depth), the bipoles at the far depth no longer receive competition from the rightmost square. They can then collinearly complete the boundaries of the leftmost square (Fig. 8d and e), which can then trigger filling-in of this square (Fig. 9b), thereby leading to a percept of unique transparency.

6. Bipole grouping in V2 interacts with the monocular contrast constraint in V1

Why are the boundaries of the rightmost square in Fig. 8b stronger than those of the leftmost square? The unique transparency image shown in Fig. 10 shows that the contrast value at region A is larger than at region B. In addition, the contrast values at C and D can be nearly equal. In these cases, the average contrast of edge AC is larger than that of BD. How, then, does the bipole whose lobes are on BD win over those on AC, as required by Figs. 8 and 9?

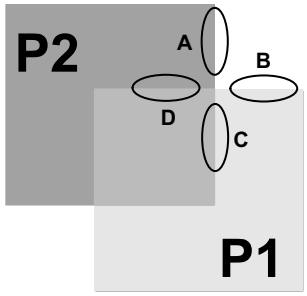

Fig. 10. Boundary BD can win over AC even if contrast AC > BD to keep the transparent surface in front. Consider Fig. 12 for the solution of this "absolute value problem".

Something more must happening to generate the proper boundary gaps, other than bipole grouping. Although the average contrast of edge AC is larger than that of BD, the contrast polarity of edge A is the same as that of the edge C, whereas the contrast polarities of B and D are opposite. Monocular polarity-specific competition in V1 therefore weakens the AC boundary, but not the BD boundary. As shown below, the competition weakens the amplitudes of inputs to the AC bipoles, but not the BD bipoles, in V2. This additional property, when combined with the other properties summarized in Fig. 8 and 9, suffices to explain all of our targeted data about transparency and neon color spreading.

7. Prediction: monocular polarity-specific competition occurs in V1 layer 4

We propose that the monocular polarity-specific competition occurs among simple cells of layer 4. Each layer 6 simple cell in Fig. 1 directly excites the corresponding layer 4 simple cell with the same contrast polarity (see also Table 1, row 3) and indirectly inhibits it via the inhibitory interneuron (Table 1, row 4). Because excitation and inhibition are approximately balanced within the on-center of the layer 4 cell, with the excitation possibly a little stronger, net excitatory modulation by layer 6 of its layer 4 on-center can occur. The layer 4 cell is also activated to suprathreshold values by direct LGN inputs (Table 1, row 1). In addition, off-surround inhibition from layer 6 to layer 4 extends to the coaxial flankers of layer 4 simple cells that have the same polarity response; see also Table 1, row 4. We predict that the latter circuit embodies monocular polarity-specific competition.

As noted above, in the unique transparency stimulus of Fig. 10, A and C have the same contrast polarity, hence they compete, so the simple cell activities in this region become weaker. Because regions B and D have opposite contrast polarity, they do not compete. Their corresponding simple cell activities are actually stronger than in the case that either boundary B or D would have continued uniformly without crossing a junction. This is because a uniform edge has the same polarity of contrast along its border, which activates the same-polarity competition pathway. The reversal of polarity from B to D frees the corresponding simple cells from continuous edge-induced inhibition and thereby makes the boundary signal around the junction zone stronger than in the case wherein a uniform edge continues. This strong BD boundary can win the orientational competition over the weakened AC boundary at the bipole cells in V2, despite the fact that the average absolute contrast of AC is greater than that of BD. The Results section will also show that these mechanisms correctly stratify the bistable and non-transparent cases.

The same mechanisms are sufficient to explain data about neon color spreading or blockade. Fig. 11a shows that the desired situation is the winning of the bipole grouping along AC over BD even if the average contrast value along BD is greater than AC (note around C, there is no contrastive edge). Monocular polarity-specific competition helps to solve this problem: Boundary A is freed from same polarity-specific competition because it ends after crossing BD, and thereby gets even stronger. However, there is polarity-specific competition within BD. The strengthening of A through discontinuation and the weakening of BD through polarity-specific competition enable bipoles which form an illusory contour by grouping AC to win over BD through orientational competition.

The same sort of hypothesis can successfully explain the blocked neon case of Fig. 11b: Boundary BD uses its bipole grouping advantage to win even if the contrast value at A is greater than at D. This is because opposite polarities B and D do not compete.

The prediction of like-polarity competition is consistent with data of Polat and Sagi (1993), in which the

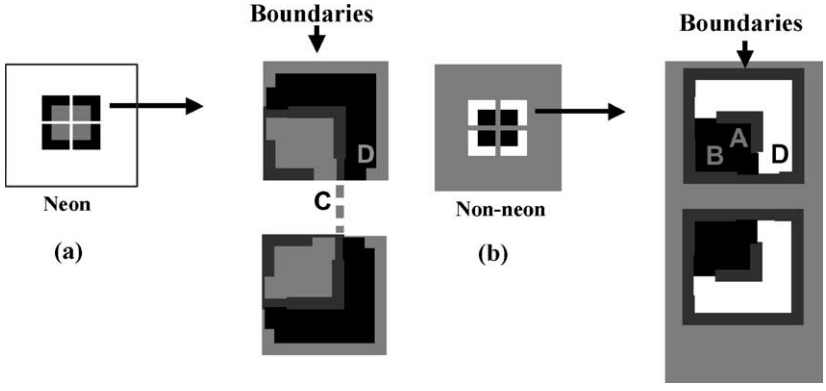

Fig. 11. Neon and no-neon cases: Boundary AC can win even when contrast D exceeds contrast A. Polarity-specific competition between B and D allows boundary AC to win. (b) Boundary BD can win even when contrast A exceeds D. Opposite-polarity B and D contrasts do not compete. Boundaries are shown schematically as grey edges.

detection threshold of a Gabor patch flanked by two patches with the same contrast polarity increases when the flankers get nearer to the target. In their experiment, the flanker contrasts were in phase with the target contrast, equivalent to a like-polarity condition. It remains to be tested via direct recording in V1 what happens if the flanker contrast and the target contrast are spatially out of phase. One has to be cautious even to draw the conclusion that in the out-of-phase case, or opposite polarity case, the raised threshold effect will be less, because polarity-pooled cells of V2 (among other cells) may modulate the predicted V1 effects.

8. Same ocularity of contrast can induce neon

The combination of monocular polarity-specific competition in V1 and binocular contrast-invariant bipole grouping in V2 can also explain the Takeichi et al. (1992) data. In the no-neon case of Fig. 4b, the different ocularity of the contrasts bypasses the monocular polarity-specific competition in V1. The same polarity (gray-white) of the right panel is thus not adjacent to the same polarity (black-white) of the left panel to activate this competition. In the neon case of Fig. 4a, monocular polarity-specific competition contributes to boundary

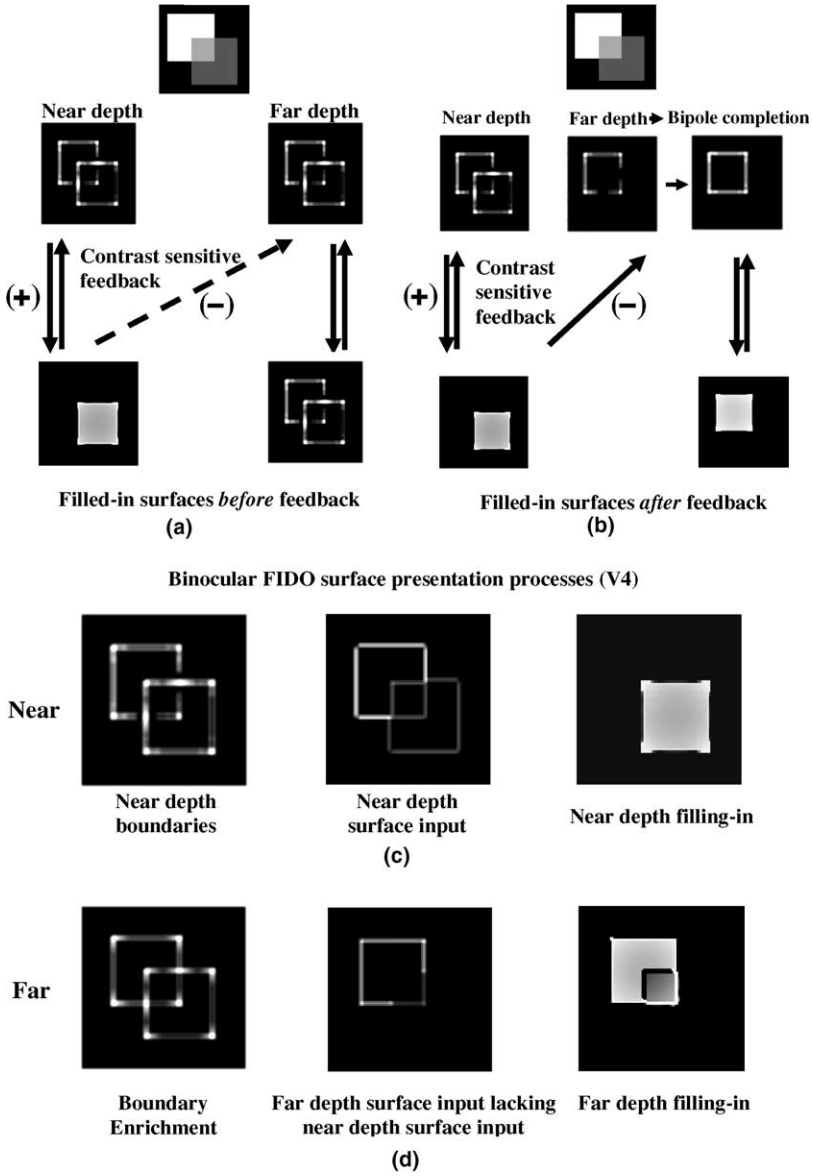

Fig. 12. (a) Before boundary pruning occurs from near-to-far, the boundary gaps in the far depth cannot be repaired. (b) After far depth boundary pruning occurs, the repaired gaps close the square boundary and allow it to contain the filling-in process. (c) The binocular FIDO stage (V4) from left to right: The near depth connected boundaries are added to the far depth boundaries. The middle panel shows that the corresponding surface inputs related to the enriched boundaries are pruned from the far depth. The right panel shows the surface filling-in of the far depth. See the text for full description.

gap formation in favor of the long-range bipole cooperation that completes the illusory square. The illusory square can form between inducers with different ocularities because layer 2/3 bipole grouping cells in V2 are binocular (Fig. 1). Taken together, the endgaps and binocular illusory contours can support the neon effect, as simulated below.

9. Simulation results

9.1. Simulation of unique transparency

For simplicity, the present simulations contain only two depth planes: near and far. Initially, the same boundaries occur in both depth planes (Fig. 12a and Appendix A.4,A.5,A.6,A.7,A.8). As described in Fig. 9a, the boundary of the rightmost square is intact and of the leftmost square has gaps. Surface filling-in is contained within the connected boundary and flows out of the gaps in the broken boundary (Appendix A.9,A.10,A.11,A.12). Fig. 12a shows the situation before the contrast-sensitive feedback takes place from the connected near surface to the far depth boundaries (Appendix A.7 and A.10). 3D LAMINART simulations of 3D planar surface percepts with more depth planes in Grossberg and Howe (2003) and Grossberg and Swaminathan (2004) show that the present simplification generalizes.

Fig. 12b shows that the analysis in Fig. 9b works; namely, after contrast-sensitive surface-to-boundary feedback in V2, the far boundary of the successfully filled-in near surface is pruned. This frees the bipole grouping kernels to repair the remaining far boundary gaps (Fig. 12b and Appendix A.8). Now surface filling-in at the far depth can be contained in this closed boundary.

In Fig. 12c, the processes involved in the Binocular Surfaces stage in V4 are shown. The near depth replicates the boundary and filled-in surface of Fig. 12b; see Fig. 12c. However, the situation at the far depth in V4 differs from that in V2 (compare Appendix A.9 and A.12). In the leftmost panel of Fig. 12d, the boundary of the successfully filled-in surface at the near depth is added to the boundary at the far depth (boundary enrichment). In addition, the surface inputs corresponding to the far boundaries are pruned from the far depth (surface pruning). In the rightmost panel, the resultant surface and boundary interaction within the Binocular Surfaces stage is shown. As can be seen, the weaker contrast of the lower-right part of the square, along with the separation of this part from the rest of the square by the boundary enrichment process, result in a weaker surface activity (rightmost panel of Fig. 12d). The latter surface activity is behind the near surface, hence gives rise to the transparency percept again. This weaker contrast illustrates how contrasts can be stratified across multiple depths.

9.2. Bistable transparency simulation

In the bistable transparency case (Fig. 2b), both stems of the X-junction preserve polarity. Due to polarity-specific competition (Appendix A.3), both generate weak boundaries. If the contrasts of both X-junctions are balanced, then their bipoles (Appendix A.8) cannot generate boundary gaps. Then the image in Fig. 2b may result in a non-stratified percept with a small square in the middle and two flanking L shapes. However, if attention shifts between the edges of the X-junction, or their corresponding surface regions, then bistable endgaps and bistable transparency can occur, because attention can favor one of the boundaries. Attention is simulated as top-down Gaussian activation to layer 6 of V1 (Fig. 13c, Appendix A.2). Layer 6, in turn, positively modulates layer 4 activation (Fig. 13c, Appendix Appendix A.3). Activation of layer 4 in favor of any boundary enables it to win the orientational competition (Appendix A.6) and to push its surface to the near depth plane.

9.3. Non-transparent simulation

A double polarity-reversing X-junction (Fig. 2c) generates strong boundary signals around X-junctions. Ori-

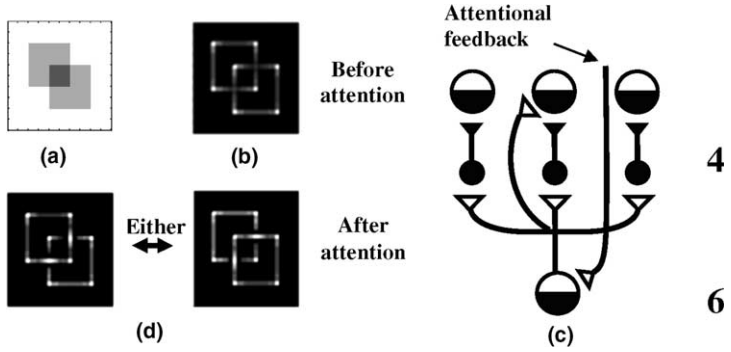

Fig. 13. In the bistable transparency case (a), the same polarity along both stems of the X-junctions makes their boundaries weak and unable to win over the other (b). Positive modulatory attentional feedback (c) to either of the stems makes it win over the other (d). See the text for details.

entational competition here too cannot generate gaps along either of them. Because both stem boundaries are strong due to the lack of polarity-specific competition, subliminal attentional boundary enhancement in favor of either stem cannot make it win over the other one, consistent with the greater effect of attention on weak than strong groupings.

The illuminant-discounted surface input successfully fills-in all the closed contours, so contrast-sensitive surface-to-boundary feedback (Appendix A.7 and A.10) prunes all the boundary copies in the far depth; hence, no boundary signals remain there. All surfaces hereby form in one depth plane with no surface representation behind the overlap region, as shown in Fig. 14, so there is no percept of transparency.

9.4. Neon simulation

In the neon case of Fig. 3a and Fig. 15a, monocular like-polarity competition (Appendix A.3) enables the illusory square to form, as was proposed in Fig. 11a. The illusory square interpolates the boundary gaps. A square surface fills-in at the near depth plane. Then contrast-sensitive surface-to-boundary feedback prunes the square boundary from the far depth plane. Boundary completion can then form four small square boundaries at the far depth plane, which can then fill-in.

The simulation clarifies the perceptual experience that the surface quality of the neon is pretty weak. In the simulation, feature contrasts occur at the four small gray square corner inducers of the illusory square. The illusory parts of the square sides do not have any surface input, because there are no contrastive edges there. These sparse inducers spread throughout the entire illusory square. This is unlike the transparency case in which the surface input exists along the whole edge of the square.

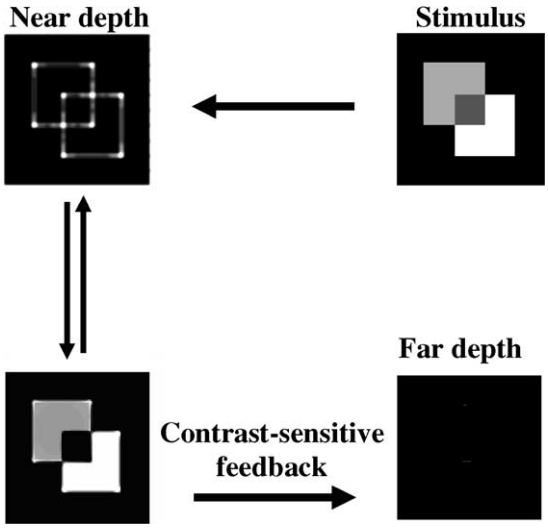

Fig. 14. In the non-transparency case, polarity reversal along both stems of X-junction leads to strong boundaries that can resist orientational competition. Attention to either boundary cannot break the other strong stem. Therefore, all closed boundaries are filled-in at the same depth plane. See text for more details.

In Fig. 15b, the simulation of the binocular surface stage (Appendix A.12) is shown. The leftmost panel shows the boundary enrichment at the far depth. The surface inputs corresponding to the near connected boundaries are pruned from the far depth surface input (middle panel). The filling-in of the pruned surface input within the enriched boundaries is shown in the right panel. The far depth surface representation is not different qualitatively at the Monocular and binocular surfaces, because the small corner square surface inputs are intact at the far depth after surface input pruning.

9.5. Non-neon simulation

Fig. 16 shows the effect of polarity reversal along the T-junctions in strengthening the boundaries corresponding to the top of the T-junction, and in not allowing the perpendicular bipole grouping to take place, as schematized in Fig. 11b. As a result, the whole surface representation is on one depth plane, much as in the non-transparent simulation in Fig. 14.

9.6. Dichoptic neon simulation

In the neon split case (Fig. 4a) because the whole contrast exists within each monocular inducer, suitable boundary gaps will be generated and binocular long-range grouping can bridge between inducers with the opposite ocularity (Fig. 17). The rest of the process is the same as in the neon case of Fig. 15.

9.7. Dichoptic non-neon split contrast simulation

Due to the different ocularity of the contrast components in this case (Fig. 4b), the boundaries around the line ends get stronger. The pooling of polarity and ocularity at layer 2/3 of V2 (Appendix A.8) results in strong boundary signals perpendicular to the orientations of the illusory square that forms in the neon case. Orientation competition (Appendix A.8) prevents boundary gaps and illusory contour formation from occurring (Fig. 18).

10. Discussion: supportive data and new predictions

10.1. Physiological and anatomical data that support the model

Neurophysiological and anatomical data support every processing stage of the model (Table 1), including its laminar interpretation. The model does not include cortical areas V3 and V3A, which are known to be involved in depth perception (Backus, Fleet, Parker, &

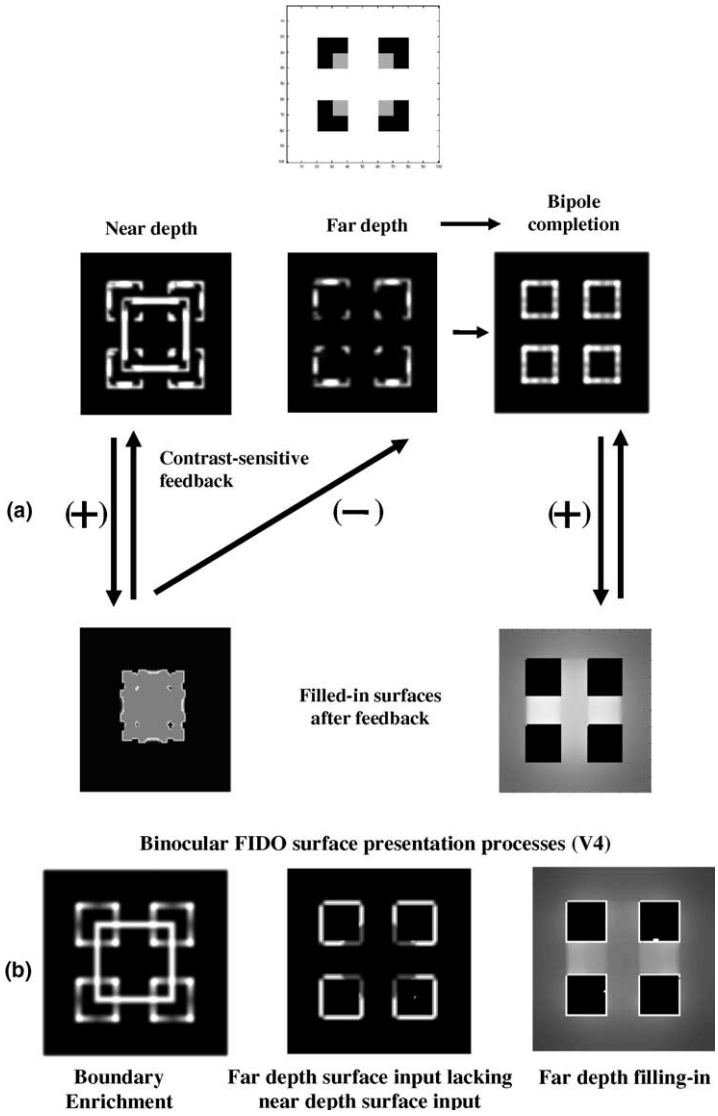

Fig. 15. (a) In the neon case, the preserved polarity along the T-junction tops weakens the top boundary signals and enables boundary gaps to form via orientational competition. These gaps create a suitable condition for long-range grouping whereby the middle square illusory boundary forms. This middle square fills-in successfully and after pruning the corresponding boundaries from the far depth, four small square boundaries are repaired by long-range grouping after being released from orientational competition by the middle square boundaries. Filling-in of the four squares can then occur behind the middle square. (b) Left panel shows that, at the binocular FIDO stage, the connected boundaries of the successfully filled-in surface at near depth are added to the boundaries at the far depth (boundary enrichment). The surface inputs corresponding to the enriched boundaries are removed from far depth via surface pruning (middle panel). The surface filling-in within the enriched boundaries by the pruned surface input represents the four corner squares at the far depth (right panel).

Heeger, 2001; Tsao et al., 2003). These areas are not required to simulate the present data. The function of area V3A is controversial. Studies propose that it is variously involved in relative disparity (Backus et al., 2001), saccades (Nakamura & Colby, 2000a, 2000b) and grasping hand movements (Nakamura et al., 2001). As a further complication, there is evidence showing that the function of macaque V3A is different from that of human V3A (Tootell et al., 1997). These areas may be required when the present model is combined with mechanisms for looking, reaching and grasping.

10.2. Predictions and the explanatory power of the model

All of the model processing stages have explicit neural labels, so their functional properties constitute testable predictions. Many such predictions have been tested with positive results; see Dresp and Grossberg (1997), Dresp and Grossberg (1999), Dresp, Durand, and Grossberg (2002), Howe (2000), Howe and Watanabe (2003), Raizada and Grossberg (2003), and Yazdanbakhsh and Watanabe (2004) for recent examples.

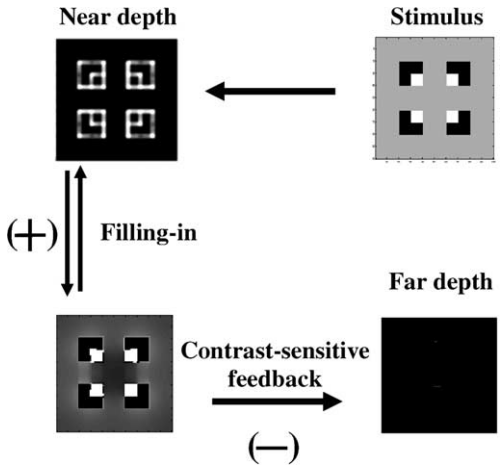

Fig. 16. In the non-neon case, opposite polarities along the tops of the T-junctions strengthen the top boundaries, which in turn block the long-range grouping by orientational competition.

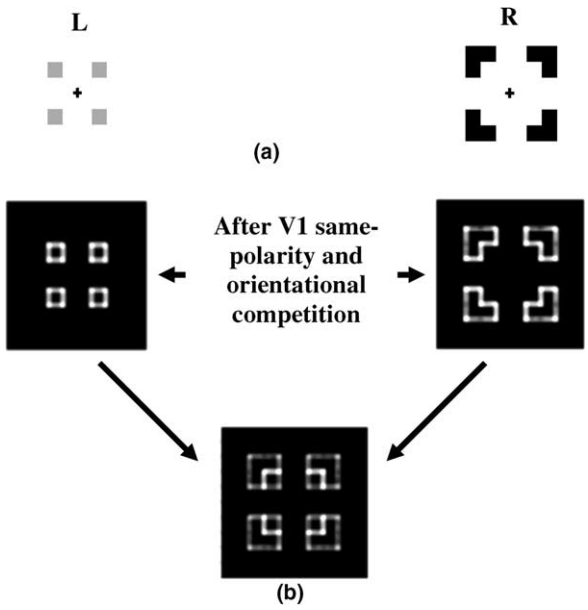

Fig. 18. In the dichoptic non-neon case, the different ocularity of the contrast components (a) bypasses the polarity-specific competition so that no endgaps are formed (b). Binocular long-range grouping to form a middle illusory square is blocked by strong perpendicular boundaries (b). See text for details.

The stimuli that generate transparency and neon color spreading are rare in natural conditions, but they illuminate constraints on visual system strategies for depth stratification that have evolved in natural environments. In particular, the monocular like-polarity constraint is predicted to be realized in the monocular circuits of layers 6 and 4 of V1. The model shows how this constraint coexists with the facts that long-range grouping can pool over opposite contrast polarities and in response to dichoptic inputs. The latter properties are realized by layer 2/3 of V2.

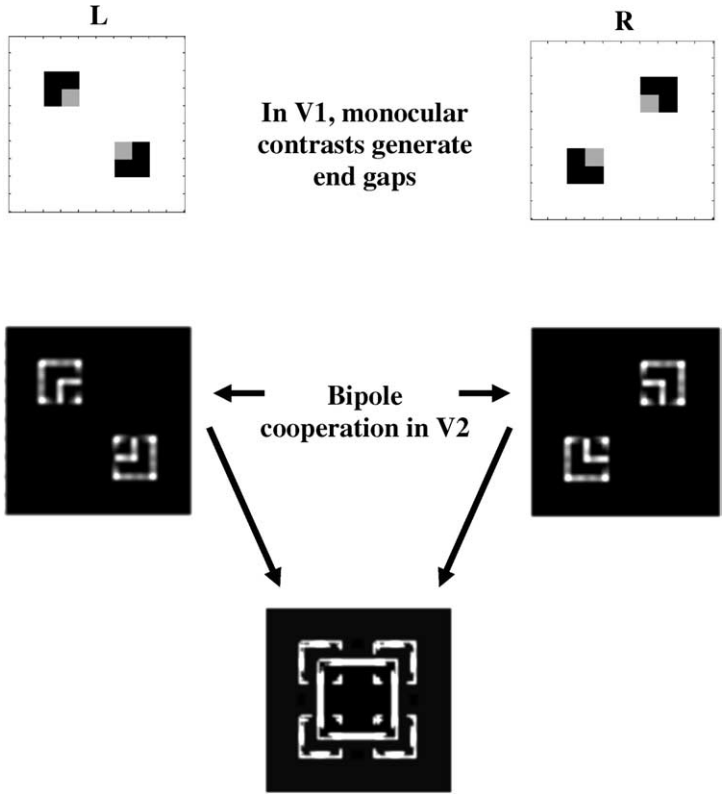

Fig. 17. In the dichoptic neon case, the presentation of the whole contrast to each eye generates boundary endgaps. Due to the binocularity of long-range grouping, the middle illusory square boundary can form. Hence neon can be generated. See text for details.

The long-range grouping process in layer 2/3 of V2 has a clear ecological value; see Fig. 5. Can the same be said for monocular polarity-specific competition in layer 6-to-4 of V1? Earlier analysis has shown that the layer 6-to-4 competition has at least three useful functions (Grossberg, 1999a): (1) it contrast-normalizes the responses of layer 4 cells to bottom-up inputs; (2) it assures that the correct groupings are selected via layer 2/3-6-4-2/3 feedback without losing their analog sensitivity to inputs; and (3) it maintains an approximate balance between excitation and inhibition in the layer 6-to-4 on-center that enables top-down attention to modulate layer 4 cells, as in Fig. 13c. These properties do not, however, require the polarity-specificity of layer 4 competition. How does this constraint arise? Grossberg and Williamson (2001) simulated how the layer 6-to-4 competition and the layer 2/3 long-range grouping connections develop. Their study showed how the approximate balance between excitation and inhibition in the layer 6-to-4 on center could develop, and that, if the excitation or inhibition got too strong, then model development did not stabilize.

The developmental and learning laws that achieve the desired stabilizing balance also create an inhibitory kernel around layer 4 cells that links cells which code the same collinear orientation, since "cells that fire together wire together". Under natural viewing conditions, objects typically have the same orientation *and* the same contrast polarity for a considerable distance along their edges. One would therefore expect monocular like-polarity inhibitory kernels to develop.

This analysis leads to new experimental questions and predictions that link properties (1)–(3) above with issues about developmental stability and transparency. In particular, what happens to these inhibitory kernels if animals are reared in an artificial environment composed of textures whose polarities reverse at frequent intervals across space? Do these animals develop inhibitory kernels that violate the like-polarity constraint? Do relative contrast differences per se then determine their percepts? Do they see transparency and neon percepts differently than we do?

When the like-polarity constraint is realized within the 3D LAMINART model, it provides a mechanistic explanation of the classical Metelli rules for when a transparent percept will be generated. In particular, Beck et al. (1984) and Metelli (1974) showed that transparency occurs when (1) "the overlying of the transparent surface does not change the order of the lightness values", and (2) "the lightness difference within the transparent area must be less than the lightness difference outside the transparent area". Because of like-polarity competition, constraint (1) can break the boundary of the non-transparent surface and leave the transparent one intact. Like-polarity competition supplemented by orientational competition (Appendix A.8) generates a larger gap on the boundary of the non-transparent surface inside the transparent area than outside of it if constraint (2) is obeyed. The larger gap leads to a more uniform spreading of surface activity within the transparent area. This is consistent with the percept: the overlaying transparent surface has a uniform surface quality.

Appendix A. 3D LAMINART equations

The main model equations are listed here. See http://cns.bu.edu/Profiles/Grossberg for a complete description of equations, parameters, and simulation methods.

A.1. Retinal/LGN processing and outputs to V1

Notation $I_{pq}^{\mathrm{L/R}}$ denotes the visual input to the lumped retina and LGN processing stages of the left (L) or right (R) eye at location (p,q). Contrast-sensitive ON cell activity $x_{ij}^{\mathrm{L/R}+}$ obeys an on-center ($C_{ij}^{\mathrm{L/R}}$) off-surround ($S_{ij}^{\mathrm{L/R}}$) membrane equation

$$\frac{\mathrm{d}x_{ij}^{\mathrm{L/R}+}}{\mathrm{d}t} = -x_{ij}^{\mathrm{L/R}+} + \left(U_1 - x_{ij}^{\mathrm{L/R}+}\right) C_{ij}^{\mathrm{L/R}} - \left(x_{ij}^{\mathrm{L/R}+} + L_1\right) S_{ij}^{\mathrm{L/R}}. \tag{1}$$

Contrast-sensitive OFF cell kernels are reversed (Grossberg & Kelly, 1999):

$$\frac{\mathrm{d}x_{ij}^{\mathrm{L/R}-}}{\mathrm{d}t} = -x_{ij}^{\mathrm{L/R}-} + (U_1 - x_{ij}^{\mathrm{L/R}-}) S_{ij}^{\mathrm{L/R}} - (x_{ij}^{\mathrm{L/R}-} + L_1) C_{ij}^{\mathrm{L/R}}, \tag{2}$$

where $C_{ij}^{\mathrm{L/R}} = \left[\sum_{pq} I_{pq}^{\mathrm{L/R}} C_{pqij}^{(k)}\right]^+$, $S_{ij}^{\mathrm{L/R}} = \left[\sum_{pq} I_{pq}^{\mathrm{L/R}} S_{pqij}^{(k)}\right]^+$, and the kernels $C_{pqij}^{(k)}$ and $S_{pqij}^{(k)}$ are Gaussian.

ON and OFF cells compete to yield the following ON and OFF output signals to V1:

$$X_{ij}^{\mathrm{L/R}+} = [x_{ij}^{\mathrm{L/R}+} - x_{ij}^{\mathrm{L/R}-}]^+,$$
$$X_{ij}^{\mathrm{L/R}-} = [x_{ij}^{\mathrm{L/R}-} - x_{ij}^{\mathrm{L/R}+}]^+. \tag{3}$$

These output signals give rise to oriented and polarity-sensitive inputs $S_{ijk}^{\mathrm{L/R}} = [\sum_{pq} X_{ij}^{\mathrm{L/R}+} D_{pqij}^{(k)}]^+$ to V1 from LGN, at V1 position (i,j) and orientation k, originating from the left (L) or right (R) eye, where kernel $D_{pqij}^{(k)}$ is defined by a difference-of-shifted-Gaussians.

A.2. Layer 6 of V1

Cell activity $x_{ijk}^{(1,\mathrm{L/R})}$ of layer 6 of V1 at position (i,j) with left/right (L/R) ocularity and orientation index k is given by:

$$\frac{\mathrm{d}}{\mathrm{d}t} x_{ijk}^{(1,\mathrm{L/R})} = -x_{ijk}^{(1,\mathrm{L/R})} + \left(1 - x_{ijk}^{(1,\mathrm{L/R})}\right)\left(S_{ijk}^{\mathrm{L/R}} + \sum_{pq} A_{ij}^{pq}\right). \tag{4}$$

Attentional feedback $\sum_{pq} A_{ij}^{pq}$ in (4) is defined by a sum of Gaussians.

A.3. V1 layer 4: monocular simple cells and like-polarity competition

The monocular simple cell activity of layer 4, $y_{ijk}^{(1,L/R)}$, is given by

$$\frac{d}{dt}y_{ijk}^{(1,L/R)} = -y_{ijk}^{(1,L/R)} + \left(1 - y_{ijk}^{(1,L/R)}\right)\left(S_{ijk}^{L/R} + \eta x_{ijk}^{(1,L/R)}\right) - \left(y_{ijk}^{(1,L/R)} + 1\right)\sum_{pq\in N_{ij}} W_{pqijk} m_{pq}^{L/R}, \quad (5)$$

where the inhibitory interneuronal activities, $m_{pq}^{L/R}$, deliver like-polarity competition from V1 layer 6. The kernel for the vertical orientations is an anisotropic Gaussian; see Fig. A.1a. The inhibitory interneuron activity, $m_{ijk}^{L/R}$, obeys:

$$\frac{d}{dt}m_{ijk}^{L/R} = -m_{ijk}^{L/R} + \eta^{-} x_{ijk}^{(1,L/R)} - m_{ijk}^{L/R}\sum_{pq\in N_{ij}} W_{pqijk}^{-} m_{pq}^{L/R}. \quad (6)$$

Kernel W_{pqijk}^{-} is a linearly scaled version of W_{pqijk} in (5); namely, $W_{pqijk}^{-} = 0.15\ W_{pqijk}$. Inhibitory interneurons hereby inhibit each other to normalize the total inhibition.

A.4. V1 layer 3B: vertical binocular simple cells

Vertically oriented layer 3B cells with activity $b_{ijkd}^{(1,B)}$, binocularly fuse layer 4 vertically oriented like-polarity monocular simple cell inputs

$$b_{ijkd}^{(1,B)} = \frac{1}{\gamma_1}\left([y_{(i-s)jk}^{(1,R)}]^{+} + [y_{(i+s)jk}^{(1,L)}]^{+} - \alpha\left([q_{ijkd}^{L}]^{+} + [q_{ijrd}^{L}]^{+} + [q_{ijkd}^{R}]^{+} + [q_{ijrd}^{R}]^{+}\right)\right). \quad (7)$$

The binocular simple cell $b_{ijkd}^{(1,B)}$ is excited by layer 4 simple cells of both ocularities with the same polarity (index k in $[y_{(i-s)jk}^{(1,R)}]^{+} + [y_{(i+s)jk}^{(1,L)}]^{+}$). Index d shows the depth plane, $d = 1$ for the near depth and $d = 2$ for the far depth. The parameters $i + s$ and $i - s$ indicate the shifted monocular positions corresponding to the binocular positions i in each depth plane. The retinal images of both eyes can be projected back along the line of sight onto the fixation plane ($d = 1$, Fig. A.1c).

The simple cell activity $b_{ijkd}^{(1,B)}$ is inhibited by all like-oriented inhibitory interneurons at their position (i,j), including those with opposite polarities (indices k and r) via terms $[q_{ijkd}^{L}]^{+} + [q_{ijrd}^{L}]^{+}$ and $[q_{ijkd}^{R}]^{+} + [q_{ijrd}^{R}]^{+}$ in (7). The left inhibitory interneurons obey:

$$\frac{dq_{ijkd}^{L}}{dt} = -\gamma_2 q_{ijkd}^{L} + [y_{(i+s)jk}^{(1,L)}]^{+} - \beta\left([q_{ijkd}^{R}]^{+} + [q_{ijrd}^{R}]^{+} + [q_{ijrd}^{L}]^{+}\right). \quad (8)$$

The right inhibitory interneuron equation exchanges L and R superscripts. In (7), same-polarity inhibition (indicated by index k) assures that binocular simple cells obey an *obligate property* (Poggio, 1991): they are active only when they get excitatory input from both ocularities of layer 4 simple cells.

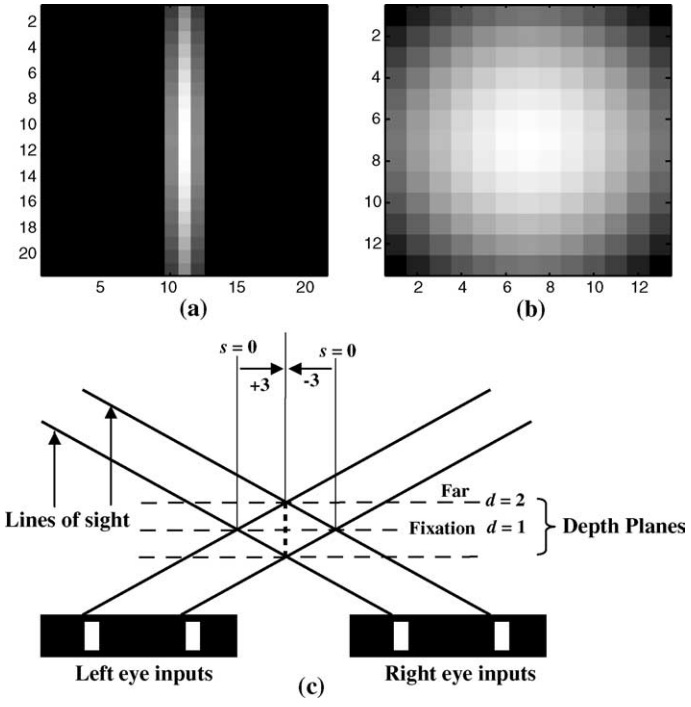

Fig. A.1. (a) Depiction of the vertical inhibitory kernel of W for Eq. (5). (b) Depiction of orientation competition kernel in Eq. (11). (c) Line of sight, allelotropic shifts, and the demonstration of different depth planes.

An additional property of the present model is the *size-disparity correlation* (Kulikowski, 1978; Richards & Kaye, 1974; Schor & Tyler, 1981; Schor & Wood, 1983; Schor et al., 1984; Tyler, 1975, 1983) whereby binocular cells can signal the presence of vertical boundaries in more than one depth plane. The present simulations consider two depth planes for simplicity.

A.5. V1 layer 3B: monocular simple cells

Monocular simple cells with activity $b_{ijk}^{(1,\mathrm{L/R})} = [y_{ijk}^{(1,\mathrm{L/R})}]^+$ are driven by monocular simple cells in layer 4 of V1 (Fig. 1).

A.6. V1 layer 2/3: complex cells

Complex cells of layer 2/3 with activity $z_{ijkd}^{(1,L/\mathrm{R/B})}$ pool opposite polarity input from layer 3B cells. Complex cells that are tuned to perpendicular orientations also compete. Monocular and binocular complex cells each carry out opposite-polarity pooling and orientational competition. Layer 2/3 complex cell activities $z_{ijrd}^{(1,\mathrm{L/R/B})}$ obey

$$\begin{aligned}\frac{\mathrm{d}}{\mathrm{d}t}z_{ijkd}^{(1,\mathrm{L/R/B})} = &-z_{ijkd}^{(1,\mathrm{L/R/B})} + (1 - z_{ijkd}^{(1,\mathrm{L/R/B})})\Big([b_{ijkd}^{(1,\mathrm{L/R/B})}]^+ \\ &+ [b_{ijrd}^{(1,\mathrm{L/R/B})}]^+\Big) - (1 + z_{ijkd}^{(1,\mathrm{L/R/B})}) \\ &\times \sum_{pq} N_{pqij}\Big([b_{pqKd}^{(1,\mathrm{L/R/B})}]^+ + [b_{pqRd}^{(1,\mathrm{L/R/B})}]^+\Big),\end{aligned} \tag{9}$$

where N_{pqij} is Gaussian and orientations K and R are perpendicular to r and k, as in Fig. A.1b.

A.7. V2 layer 4

Monocular and binocular V1 layer 2/3 cell outputs, $z_{ijk}^{(1,\mathrm{L/R})}$ and $z_{ijkd}^{(1,\mathrm{B})}$, are pooled in V2 layer 4 (Table 1, row 15). Activity $y_{ijkd}^{(2)}$ of a vertical cell ($k = 1$) V2 layer 4 cell pools both monocular and binocular V1 outputs

$$\begin{aligned}\frac{\mathrm{d}}{\mathrm{d}t}y_{ijkd}^{(2)} = &-y_{ijkd}^{(2)} + \left[z_{ijkd}^{(1,\mathrm{B})}\right]^+ + \upsilon\left(\left[z_{(i+s)jk}^{(1,\mathrm{L})}\right]^+ + \left[z_{(i-s)jk}^{(1,\mathrm{R})}\right]^+\right) \\ &- \delta\sum_{e<d}(p_{ije}^{L} + p_{ije}^{\mathrm{R}}).\end{aligned} \tag{10}$$

A horizontal cell ($k = 2$) gets only monocular outputs. The pruning signal $p_{ije}^{\mathrm{L/R}}$ from the monocular surfaces (Fig. 6, Eq. (17)) inhibits all $y_{ijkd}^{(2)}$ at farther depths ($e < d$).

A.8. V2 layer 2/3: bipole grouping cells

Bipole cell activity, $z_{ijkd}^{(2)}$, at layer 2/3 of V2 receives long-range cooperation ($Q_{ijkd}^{(1)} + Q_{ijkd}^{(2)}$) and short-range competition ($Q_{ijkd}^{\mathrm{Is}} + Q_{ijkd}^{\mathrm{Io}} + Q_{ijkd}^{\mathrm{Id}}$) inputs:

$$\begin{aligned}\frac{\mathrm{d}}{\mathrm{d}t}z_{ijkd}^{(2)} = &-z_{ijkd}^{(2)} + (1 - z_{ijkd}^{(2)})([y_{ijkd}^{(2)}]^+ + Q_{ijkd}^{(1)} + Q_{ijkd}^{(2)}) \\ &- (z_{ijkd}^{(2)} + \psi)(Q_{ijkd}^{\mathrm{Is}} + Q_{ijkd}^{\mathrm{Io}} + Q_{ijkd}^{\mathrm{Id}});\end{aligned} \tag{11}$$

see Fig. 1. The excitatory bottom-up input, $[y_{ijkd}^{(2)}]^+$, from layer 4 sums with $Q_{ijkd}^{(1)}$ and $Q_{ijkd}^{(2)}$, which convolve elongated half-Gaussian kernels $H_{pqijk}^{(v)}$ with neighboring bipole cell outputs. Inhibitory interneurons with activity s_{ijkdv} inhibit bipole cells from both sides ($v = 1, 2$) to realize inward propagation of boundary completion via term $Q_{ijkd}^{Is} = \sum_{v=1,2}[s_{ijkdv}]^+$. Inhibitory interneuron activities s_{ijkdv} get excitatory input from horizontal connections on the same side of the bipole cell and inhibitory inputs from the opposite side ($u \neq v$) at the same position (i,j):

$$\frac{\mathrm{d}}{\mathrm{d}t}s_{ijkdv} = -s_{ijkdv} + Q_{ijkd}^{(v)} - \mu_s s_{ijkdv}[s_{ijkdu}]^+. \tag{12}$$

Each bipole cell is also inhibited by other bipole orientations ($r \neq k$) around each position (i,j) via term $Q_{ijkd}^{\mathrm{Io}} = \sum_{pq,r\neq k} N_{pqij}[z_{pqrd}^{(2)} - \rho_z]^+$. A *disparity filter* inhibits false binocular matches: Each vertically oriented bipole cell with activity, $z_{ijkd}^{(2)}$, ($k = 1$) is inhibited by every other vertically oriented bipole cell that shares one of its monocular inputs (Figure A1c, oblique line of sight), or is directly in front or behind it (Figure A1c, dashed vertical line) via term

$$\begin{aligned}Q_{ijkd}^{\mathrm{Id}} = \omega_1 \sum_{d'\neq d}\Bigg(&m_{dd'}\left[z_{(i+s'-s)jkd'}^{(2)}\right]^+ \\ &+ m_{dd'}\left[z_{(i+s-s')jkd'}^{(2)}\right]^+ + \omega_2\left[z_{ijkd'}^{(2)}\right]^+\Bigg).\end{aligned} \tag{13}$$

Parameter $m_{dd'} = 1.3$ when $d = 1$ (near) and $d' = 2$ (far). Parameter $m_{dd'} = 2.8$ when $d = 2$ (far) and $d' = 1$ (near). The disparity filter in Grossberg and Howe (2003) did not include perceptual grouping. Cao and Grossberg (2004) included bipole-based 3D grouping and a disparity filter that suppresses groupings corresponding to false matches by using an equation like (13). This showed that binocular false matches can be eliminated as part of the Gestalt grouping process. Here the same process handles different data.

A.9. V2 monocular surfaces

The monocular surfaces stage responds to the following LGN inputs. The ON filling-in domain, or FIDO, receives unoriented LGN inputs $X_{ij}^{\mathrm{L/R+}}$ and the OFF FIDO receives inputs $X_{ij}^{\mathrm{L/R-}}$ both defined in (3). BCS boundary signals $Z_{ijd} = \sum_{k=1}^{2} z_{ijkd}^{(2)}$ block filling-in. They sum all orientations of bipole cell outputs at each position and depth. Filling-in dynamics obey a boundary-gated diffusion equation in which $F_{ijd}^{\mathrm{L/R,+}}$ is the monocular Left/Right ON surface signal at position (i, j) and depth d:

$$\begin{aligned}\frac{\mathrm{d}}{\mathrm{d}t}F_{ijd}^{\mathrm{L/R+}} = &-mF_{ijd}^{\mathrm{L/R+}} + \sum_{(p,q)\in N_{ij}}\left(F_{pqd}^{\mathrm{L/R+}} - F_{ijd}^{\mathrm{L/R+}}\right)P_{pqijd}^{(M)} \\ &+ X_{(i+s)j}^{\mathrm{L/R+}}.\end{aligned} \tag{14}$$

The diffusion coefficients, $P^{(M)}_{pqijd}$, are defined by

$$P^{(M)}_{pqijd} = \frac{\delta}{1 + \varepsilon(Z_{pqd} + Z_{ijd})}. \quad (15)$$

A similar equation holds for the OFF surface signal with (+) replaced by (−) everywhere.

LGN inputs are shifted along the line of sight to match their boundaries at each depth. Diffusion occurs between nearest neighbors $N_{ij} = \{(i,j-1),(i-1,j),(i+1,j),(i,j+1)\}$. OFF filling-in with activity $F^{\mathrm{L/R}-}_{ijd}$ obeys the same equation with plus signs replaced by minus signs. The monocular surfaces output is defined by a double-opponent filled-in signal

$$R^{\mathrm{L/R}}_{ijd} = \left[F^{\mathrm{L/R}+}_{ijd} - F^{\mathrm{L/R}-}_{ijd}\right]^{+} \quad (16)$$

which cancels when there is a gap in the boundary signal of an edge: ON filling-in spreads across the gap from one side of it, whereas the OFF filling-in spread across the gap from the other side.

A.10. Monocular surfaces output

Boundary pruning signals p_{ijd} from near to far depth in (17) and (18) (see Fig. 9b), are generated when filled-in activities at the monocular surfaces activate a contrast-sensitive on-center off-surround network:

$$\frac{\mathrm{d}}{\mathrm{d}t}p^{\mathrm{L/R}}_{ijd} = -\alpha_b p^{\mathrm{L/R}}_{ijd} + \left(U_b - p^{\mathrm{L/R}}_{ijd}\right)C^{\mathrm{L/R}}_{bd} - \left(L_b + p^{\mathrm{L/R}}_{ijd}\right)E^{\mathrm{L/R}}_{bd}. \quad (17)$$

The on-center $C^{\mathrm{L/R}}_{bd} = \sum_{(p,q)\in N_{ij}} C_{pq} R^{\mathrm{L/R}}_{i+p,j+q,d}$ and off-surround $E^{\mathrm{L/R}}_{bd} = \sum_{(p,q)\in N_{ij}} E_{pq} R^{\mathrm{L/R}}_{i+p,j+q,d}$ both use Gaussian kernels C_{pq} and E_{pq}.

A.11. Pruning of the binocular surfaces input

Visible surface signals occur at the binocular surfaces stage. Here, binocularly matched LGN signals from both eyes activate depth-selective filling-in domains (pathway 8 in Fig. 6). The contrast-sensitive monocular surfaces outputs from nearer depths and both eyes prune, or inhibit, redundant surface signals at the same positions and further depths (pathways 9 in Fig. 6). The activity ϕ_{ijd} of a binocular surfaces cell at position (i,j) and depth d thus obeys:

$$\frac{\mathrm{d}}{\mathrm{d}t}\phi^{+/-}_{ijd} = -\alpha_{bf}\phi^{+/-}_{ijd} + \left(U_{bf} - \phi^{+/-}_{ijd}\right)\left(X^{L+/-}_{(i+s)j} + X^{R+/-}_{(i-s)j}\right) - \left(L_{bf} + \phi^{+/-}_{ijd}\right)\sum_{e<d}\left(p^{L}_{ije} + p^{R}_{ije}\right). \quad (18)$$

A.12. Binocular surfaces from using enriched boundaries

Finally, activities $\mu^{+/-}_{ijd}$ represent the ON and OFF filled-in surface representation at the binocular surfaces stage:

$$\frac{\mathrm{d}}{\mathrm{d}t}\mu^{+/-}_{ijd} = -m\mu^{+/-}_{ijd} + \sum_{(p,q)\in N_{ij}}\left(\mu^{+/-}_{pqd} - \mu^{+/-}_{ijd}\right)P^{(\mathrm{B})}_{pqijd} + \phi^{+/-}_{ijd}. \quad (19)$$

In (19), terms $P^{(\mathrm{B})}_{pqijd}$ represent the boundary-gated permeabilities

$$P^{(\mathrm{B})}_{pqijd} = \frac{\delta}{1 + \varepsilon(\xi_{pqd} + \xi_{ijd})}. \quad (20)$$

The boundaries that gate filling-in are enriched (e.g., Fig. 12c and Fig. 15d) by adding all nearer boundaries at each position $\xi_{ijd} = \sum_{ed} Z_{ije}$. The double-opponent filled-in activity, $R^{(\mathrm{B})}_{ijd}$, represents the visible surface percept

$$R^{(\mathrm{B})}_{ijd} = \left[\mu^{+}_{ijd} - \mu^{-}_{ijd}\right]^{+}. \quad (21)$$

References

Adelson, E. H. (2000). Lightness perception and lightness illusions. In M. Gazzaniga (Ed.), *The new cognitive neurosciences* (2nd ed., pp. 339–351). Cambridge, MA: MIT Press.

Ahmed, B., Anderson, J. C., Martin, K. A. C., & Nelson, J. C. (1997). Map of the synapses onto layer 4 basket cells of the primary visual cortex of the cat. *Journal of Comparative Neurology, 380*, 230–242.

Anderson, B. L. (1997). A theory of illusory lightness and transparency in monocular and binocular images: the role of contour junctions. *Perception, 26*, 419–453.

Backus, B. T., Fleet, D. J., Parker, A. J., & Heeger, D. J. (2001). Human cortical activity correlates with stereoscopic depth perception. *Journal of Neurophysiology, 86*, 2054–2068.

Bakin, J. S., Nakayama, K., & Gilbert, C. D. (2000). Visual responses in monkey area V1 and V2 to three-dimensional surface configurations. *The Journal of Neuroscience, 20*, 8188–8198.

Beck, J., Prazdny, K., & Ivry, R. (1984). The perception of transparency with achromatic colors. *Perception and Psychophysics, 35*, 407–422.

Blasdel, G. G., & Lund, J. S. (1983). Termination of afferent axons in macaque striate cortex. *Journal of Neuroscience, 3*, 1389–1413.

Bosking, W., Zhang, Y., Schofield, B., & Fitzpatrick, D. (1997). Orientation selectivity and the arrangement of horizontal connections in tree shrew striate cortex. *Journal of Neuroscience, 17*(6), 2112–2127.

Callaway, E. M. (1998). Local circuits in primary visual cortex of the macaque monkey. *Annual Review of Neuroscience, 21*, 47–74.

Callaway, E. M., & Wiser, A. K. (1996). Contributions of individual layer 2–5 spiny neurons to local circuits in macaque primary visual cortex. *Visual Neuroscience, 13*, 907–922.

Cao, Y., & Grossberg, S. (2004). A laminar cortical model of stereopsis and 3D surface perception: Closure and da Vinci stereopsis.

Cumming, B. G., & Parker, A. J. (2000). Local disparity not perceived depth is signaled by binocular neurons in cortical area V1 of the macaque. *The Journal of Neuroscience, 20*, 4758–4767.

Dow, B. M. (1974). Function classes of cells and their laminar distribution in monkey visual cortex. *Journal of Neurophysiology, 37*, 927–946.

Dresp, B., & Grossberg, S. (1997). Contour integration across polarities and spatial gaps: From local contrast filtering to global grouping. *Vision Research, 37*, 913–924.

Dresp, B., & Grossberg, S. (1999). Spatial facilitation by color and luminance edges: boundary, surface, and attentional factors. *Vision Research, 39*, 3431–3443.

Dresp, B., Durand, S., & Grossberg, S. (2002). Depth perception from pairs of overlapping cues in pictorial displays. *Spatial Vision, 15*, 255–276.

Ferster, D., Chung, S., & Wheat, H. (1996). Orientation selectivity of thalamic input to simple cells of cat visual cortex. *Nature, 380*, 249–252.

Fitzpatrick, D., Lund, J. S., & Blasdel, G. G. (1985). Intrinsic connections of macaque striate cortex: afferent and efferent connections of lamina 4C. *Journal of Neuroscience, 5*(12), 3329–3349.

Grossberg, S. (1994). 3-D vision and figure-ground separation by visual cortex. *Perception and Psychophysics, 55*, 48–121.

Grossberg, S. (1997). Cortical dynamics of three-dimensional figure-ground perception of two-dimensional pictures. *Psychological Review, 104*, 618–658.

Grossberg, S. (1999a). How does the cerebral cortex work? Learning, attention, and grouping by the laminar circuits of visual cortex. *Spatial Vision, 12*, 163–185.

Grossberg, S. (1999b). The link between brain learning, attention, and consciousness. *Consciousness and Cognition, 8*, 1–44.

Grossberg, S. (2003). Filling-in the forms: Surface and boundary interactions in visual cortex. In L. Pessoa & P. DeWeerd (Eds.), *Filling-in: From perceptual completion to cortical reorganization* (pp. 13–37). New York: Oxford University Press.

Grossberg, S., & Howe, P. D. L. (2003). A laminar cortical model of stereopsis and three-dimensional surface perception. *Vision Research, 43*, 801–829.

Grossberg, S., & Kelly, F. (1999). Neural dynamics of binocular brightness perception. *Vision Research, 39*, 3796–3816.

Grossberg, S., & Mingolla, E. (1985a). Neural dynamics of perceptual grouping: Textures, boundaries, and emergent segmentations. *Perception and Psychophysics, 38*, 141–171.

Grossberg, S., & Mingolla, E. (1985b). Neural dynamics of form perception: Boundary completion, illusory figures, and neon color spreading. *Psychological Review, 92*, 173–211.

Grossberg, S., & Raizada, R. D. (2000). Contrast-sensitive perceptual grouping and object-based attention in the laminar circuits of primary visual cortex. *Vision Research, 40*, 1413–1432.

Grossberg, S., & Seitz, A. (2003). Laminar development of receptive fields, maps and columns in visual cortex: The coordinating role of the subplate. *Cerebral Cortex, 13*, 852–863.

Grossberg, S., & Swaminathan, G. (2004). A laminar cortical model for 3D perception of slanted and curved surfaces and of 2D images: Development, attention, and bistability. *Vision Research, 44*, 1147–1187.

Grossberg, S., & Williamson, J. R. (2001). A neural model of how horizontal and interlaminar connections of visual cortex develop into adult circuits that carry out perceptual grouping and learning. *Cerebral Cortex, 11*, 37–58.

Grossberg, S., & Yazdanbakhsh, A. (2003a). Laminar cortical dynamics of 3D surface stratification, transparency, and neon spreading. In *Proceedings of the 3rd annual meeting of the Vision Sciences Society, FR43* (p. 77).

Grossberg, S., & Yazdanbakhsh, A. (2003b). Laminar cortical mechanisms of 3D surface processing. In *Proceedings of the Society for Neuroscience 33rd annual meeting* (p. 339.5).

Hirsch, J. A., & Gilbert, C. D. (1991). Synaptic physiology of horizontal connections in the cat's visual cortex. *Journal of Neuroscience, 11*(6), 1800–1809.

Howe, P. D. (2000). A comment on the Anderson (1997), the Todorovic (1997), and the Ross and Pessoa explanations of White's effect. *Perception, 30*, 1023–1026.

Howe, P. D., & Watanabe, T. (2003). Measuring the depth induced by an opposite-luminance (but not anticorrelated) stereogram. *Perception, 32*, 415–421.

Hubel, D. H., & Livingstone, M. S. (1987). Segregation of form, color, and stereopsis in primate area 18. *The Journal of Neuroscience, 7*, 3378–3415.

Hubel, D. H., & Wiesel, T. N. (1968). Receptive fields and functional architecture of monkey striate cortex. *Journal of Physiology, 195*, 215–243.

Katz, L. C., Gilbert, C. D., & Wiesel, T. N. (1989). Local circuits and ocular dominance columns in monkey striate cortex. *The Journal of Neuroscience, 9*, 1389–1399.

Kelly, F., & Grossberg, S. (2000). Neural dynamics of 3-D surface perception: Figure-ground separation and lightness perception. *Perception and Psychophysics, 62*, 1596–1618.

Kulikowski, J. J. (1978). Limit of single vision in stereopsis depends on contour sharpness. *Nature, 275*, 126–127.

Metelli, F. (1974). The perception of transparency. *Scientific American, 230*, 90–98.

McGuire, B. A., Gilbert, C. D., Rivlin, P. K., & Wiesel, T. N. (1991). Targets of horizontal connections in macaque primary visual cortex. *Journal of Comparative Neurology, 305*(3), 370–392.

McGuire, B. A., Hornung, J. P., Gilbert, C. D., & Wiesel, T. N. (1984). Patterns of synaptic input to layer 4 of cat striate cortex. *Journal of Neuroscience, 4*, 3021–3033.

Nakamura, K., & Colby, C. L. (2000a). Visual, saccade-related, and cognitive activation of single neurons in monkey extrastriate area V3A. *Journal of Neurophysiology, 84*, 677–692.

Nakamura, K., & Colby, C. L. (2000b). Updating of the visual representation in monkey striate and extrastriate cortex during saccades. *Proceedings of the National Academy of Sciences, 99*, 4026–4031.

Nakamura, H., Kuroda, T., Wakita, M., Kusunoki, M., Kato, A., Mikami, A., Sakata, H., & Itoh, K. (2001). From three-dimensional space vision to prehensile hand movements: The lateral intraparietal area links the area V3A and the anterior intraparietal area in macaque. *The Journal of Neuroscience, 21*, 8174–8187.

Peterhans, E. (1997). Functional organization of area V2 in the awake monkey. *Cerebral Cortex, 12*, 335–357.

Poggio, G. F. (1972). Spatial properties of neurons in striate cortex of unanesthetized macaque monkey. *Investigative Ophthalmology, 11*, 369–377.

Poggio, G. F. (1991). Physiological basis of stereoscopic vision. In *Vision and visual dysfunction binocular vision* (pp. 224–238). Boston, MA: CRC.

Poggio, G. F., & Fischer, B. (1977). Binocular interaction and depth sensitivity in striate and prestriate cortex of behaving rhesus monkey. *Journal of Neurophysiology, 40*, 1392–1405.

Poggio, G. F., & Talbot, W. H. (1981). Mechanisms of static and dynamic stereopsis in foveal cortex of the rhesus monkey. *Journal of Physiology, 315*, 469–492.

Polat, U., & Sagi, D. (1993). Lateral interactions between spatial channels: suppression and facilitation revealed by lateral masking experiments. *Vision Research, 33*(7), 993–999.

Raizada, R. D., & Grossberg, S. (2003). Towards a theory of the laminar architecture of cerebral cortex: Computational clues from the visual system. *Cerebral Cortex, 13*, 100–113.

Richards, W., & Kaye, M. G. (1974). Local versus global stereopsis: two mechanisms? *Vision Research, 14*, 1345–1347.

Rockland, K. S., & Virga, A. (1990). Organization of individual cortical axons projecting from area VI (area 17) to V2 (area 18) in the macaque monkey. *Visual Neuroscience, 4*(1), 11–28.

Roe, A. W., & Ts'o, D. Y. (1997). The functional architecture of area V2 in the macaque monkey. *Cerebral Cortex, 12*, 295–333.

Schmidt, K. E., Goebel, R., Löwel, S., & Singer, W. (1997). The perceptual grouping criterion of colinearity is reflected by anisotropies of connections in the primary visual cortex. *European Journal of Neuroscience, 9*, 1083–1089.

Schor, C. M., & Tyler, C. W. (1981). Spatio-temporal properties of Panum's fusional area. *Vision Research, 21*, 683–692.

Schor, C. M., & Wood, I. (1983). Disparity range for local stereopsis as a function of luminance spatial frequency. *Vision Research, 23*, 1649–1654.

Schor, C., Wood, I., & Ogawa, J. (1984). Binocular sensory fusion is limited by spatial resolution. *Vision Research, 24*, 661–665.

Smith, E. L., Chino, Y., Ni, J., & Cheng, H. (1997). Binocular combination of contrast signals by striate cortical neurons in the monkey. *Journal of Neurophysiology, 78*, 366–382.

Stratford, K. J., Tarczy-Hornoch, K., Martin, K. A. C., Bannister, N. J., & Jack, J. J. B. (1996). Excitatory synaptic inputs to spiny stellate cells in cat visual cortex. *Nature, 382*, 258–261.

Takeichi, H., Shimojo, S., & Watanabe, T. (1992). Neon flank and illusory contour: interaction between the two processes leads to color filling-in. *Perception, 21*, 313–324.

Tamas, G., Somogyi, P., & Buhl, E. H. (1998). Differentially interconnected networks of GABAergic interneurons in the visual cortex of the cat. *Journal of Neuroscience, 18*(11), 4255–4270.

Tootell, R. B. H., Mendola, J. D., Hadjikhani, N. K., Ledden, P. J., Liu, A. K., Reppas, J. B., Sereno, M. I., & Dale, A. M. (1997). Functional analysis of V3A and related areas in human visual cortex. *The Journal of Neuroscience, 17*, 7060–7078.

Tsao, D. Y., Vanduffel, W., Sasaki, Y., Fize, D., Knutsen, T. A., Mandeville, J. B., Wald, L. L., Dale, A. M., Rosen, B. R., VanEssen, D. C., Livingstone, M. S., Orban, G. A., & Tootell, R. B. (2003). Stereopsis activates V3A and caudal intraparietal areas in macaques and humans. *Neuron, 39*, 555–568.

Tucker, T. R., & Katz, L. C. (2003a). Recruitment of local inhibitory networks by horizontal connections in layer 2/3 of ferret visual cortex. *Journal of Neurophysiology, 89*, 501–512.

Tucker, T. R., & Katz, L. C. (2003b). Spatiotemporal patterns of excitation and inhibition evoked by the horizontal network in layer 2/3 of ferret visual cortex. *Journal of Neurophysiology, 89*, 488–500.

Tyler, C. W. (1975). Spatial organization of binocular disparity sensitivity. *Vision Research, 15*, 583–590.

Tyler, C. W. (1983). Sensory processing of binocular disparity. In C. M. Schor & K. J. Cuiffreda (Eds.), *Vergence eye movements* (pp. 199–295). Boston: Butterworths.

Van Essen, D. C., Newsome, W. T., Maunsell, J. H., & Bixby, J. L. (1986). The projections from striate cortex (V1) to areas V2 and V3 in the macaque monkey: asymmetries, areal boundaries, and patchy connections. *Journal of Comparitive Neurology, 244*(4), 451–480.

von der Heydt, R., Zhou, H., & Friedman, H. S. (2000). Representation of stereoscopic edges in monkey visual cortex. *Vision Research, 40*, 1955–1967.

Watanabe, T., & Cavanagh, P. (1993a). Surface decomposition accompanying the perception of transparency. *Spatial Vision, 7*, 95–111.

Watanabe, T., & Cavanagh, P. (1993b). Transparent surfaces defined by implicit X junctions. *Vision Research, 33*, 2339–2346.

Yazdanbakhsh, A., & Watanabe, T. (2004). Asymmetry between horizontal and vertical illusory lines in determining the depth of their embedded surface. *Vision Research, 44*, 2621–2627.